Available online at www.sciencedirect.com
SCIENCE DIRECT
Applied Catalysis B: Environmental 61 (2005) 114–119
APPLIED CATALYSIS B: ENVIRONMENTAL
www.elsevier.com/locate/apcatb

Synthesis and characterization of manganese oxides employed in VOCs abatement

Luciano Lamaita, Miguel A. Peluso, Jorge E. Sambeth *, Horacio J. Thomas

Centro de Investigación y Desarrollo en Ciencias Aplicadas (CINDECA) "Dr. Jorge J. Ronco"—UNLP, CONICET—47 No 257 (B1900AJK) La Plata, Buenos Aires, Argentina

Received 10 October 2004; received in revised form 24 March 2005; accepted 30 March 2005
Available online 25 May 2005

Abstract

Two MnO_2 were prepared by different methods: (i) $MnCO_3$ decomposition; and (ii) oxidation of acid $MnSO_4$ solution. The combined use of X-ray diffraction (XRD), DRIFTS, DRS–UV–vis and TGA techniques revealed: (i) the presence of Mn^{4+}–Mn^{3+}; (ii) a poor crystallinity; and (iii) OH species at temperatures higher than 200 °C.

The catalysts were tested in the complete oxidation of ethanol to carbon dioxide and water, and the reaction results showed that the catalytic activity of both samples were larger than MnO_2 (pyrolusite, β-MnO_2) and Mn_2O_3 (like bixbyite) oxides. The high activity of the prepared oxides can be related to the simultaneous presence of Mn^{3+} and Mn^{4+} ions and OH^- species generated by Mn^{4+} vacancies. In addition, in situ DRIFT spectroscopy demonstrated a different mechanism of adsorption-reaction of ethanol between the two synthesized manganese oxides.

Keywords: γ-MnO_2 nsutite; Manganese oxides; DRIFTS; Ethanol oxidation; VOCs

1. Introduction

Among the transition metal dioxides, MnO_2 probably exhibits the largest number of polymorph structures. Pyrolusite (β-MnO_2) is the most stable polymorph of manganese dioxide and has the structure of rutile [1]. Ramsdellite (R-MnO_2) is closely related to rutile except for the fact that double chains replace the single chains of edge—sharing octahedra [2] and nsutite or γ-MnO_2 has a highly disordered structure and has been described as an intergrowth of elements of pyrolusite and ramsdelllite [3].

Manganese dioxides can be classified according to the number of MnO_6 units and the number of MnO_6 octahedral chains between two basal layers to form tunnel openings. They are usually symbolized T(m, n) where n and m stand for the dimension of the tunnels in the two directions perpendicular to the chains of edge-sharing octahedra [4]. Thus, pyrolusite is T(1, 1) and ramsdellite is T(1, 2), so that γ-MnO_2 could be represented as T(1, 1)–T(1, 2) intergrowths.

Among the various polymorphs of MnO_2 reported in the literature (Chabre and Pannetier [4] have reported about 14 modifications) the γ-MnO_2 (nsutite) is the best-known MnO_2 polymorph used by the battery industry. γ-MnO_2 has been extensively investigated for its important application as cathode material for dry cells. According to McLean et al. [5], structural and chemical defects are responsible for electrochemical properties by the H^+ insertion and increasing the Fermi Level energy. The Volkenshtein Electronic Theory [6] states that the catalytic activity is a function of the electronic properties of solids, so the γ-MnO_2 phase could be an excellent catalyst.

In this sense, Lahousse et al. [7] and Peluso et al. [8] have shown that the γ-MnO_2 and one sample of Mn^{3+}/γ-MnO_2, respectively, are very suitable for VOC's removal catalyst.

The aims of this paper are: (1) to characterize γ-MnO_2 catalysts prepared by different methods of synthesis; (2) to study the catalytic activity in the complete oxidation of ethanol to carbon dioxide and water, and to correlate this

* Corresponding author. Fax: +54 221 425 4277.
E-mail address: sambeth@quimica.unlp.edu.ar (J.E. Sambeth).

0926-3373/$ – see front matter © 2005 Elsevier B.V. All rights reserved.
doi:10.1016/j.apcatb.2005.03.014

activity to the structural properties of the catalysts; and (3) to propose a possible adsorption–oxidation mechanism.

2. Experimental

2.1. Sample preparation

Four manganese oxide samples were used in this work. Two of them were prepared in order to obtain the γ-MnO_2 phase. In a first attempt to obtain this phase, $MnCO_3$ (Riedel de Haen RG) was oxidized at 500 °C under flowing oxygen (50 cm^3/min) with a heat rate of 20 °C min^{-1} [8]. This oxide is named hereinafter M1.

The second manganese oxide (M2) used in this work was prepared by the Netto et al. procedure [9]. A solution of $MnSO_4 \cdot H_2O$ dissolved in 3 M H_2SO_4 was oxidized with flowing oxygen (30 cm^3/min). pH was raised up to 3 with NaOH. After being filtered and washed with deionised water, the oxide was dried at 100 °C for 24 h.

For the purpose of comparison, a commercial reagent grade MnO_2 (Baker 99.9%), named M3, has been investigated. Finally, a synthetic pyrolusite (M4) prepared by thermal decomposition of solid $Mn(NO_3)_2 \cdot 4H_2O$ was also studied [10].

The list of the oxides, together with the relative notation, is presented in Table 1.

2.2. Characterization

The structure of the studied samples was characterized through X-ray diffraction (XRD) by using a Phillips PW 1390 instrument with Ni-filtered Cu Kα radiation (λ = 1.540589 Å). The diffraction patterns were taken at room temperature in the range $5 < 2\theta < 70°$. For phase identification purposes, the JCPDS database of reference compounds was used [11].

The BET specific surface areas were measured by N_2 adsorption at the liquid nitrogen temperature (77 K) in a Micromeritics Accussorb 2100 D sorptometer.

DRIFTS spectra were obtained in a Bruker IFS66 infrared spectrometer with a KBr optics and DTGS detector in the 600–4000 cm^{-1} range. An environmental DRIFTS chamber equipped with KBr window (Spectra Tech 0030-103), allowing in situ treatments up to 300 °C and 1 atm was coupled to the spectrometer. The spectra were obtained by co-adding 200 scans collected at 4 cm^{-1}.

Table 1
BET specific surface areas of the manganese oxides prepared in this study

Sample	MnO_x precursor	BET specific area (m^2 g^{-1})
M1	$MnCO_3$	11
M2	$MnSO_4 \cdot H_2O$	55
M3[a]	–	0.1
M4	$Mn(NO_3)_2 \cdot 4H_2O$	6.1

[a] MnO_2 baker 99%.

The DRS–UV–vis spectra were recorded on a Cary 2300 spectrophotometer in the region 200–2000 nm.

Thermal analyses (TG) of the catalysts were performed on a DTA-TG 50 Shimadzu analyzer between room temperature and 900 °C; small portions (14–16 mg) of the samples were used at 10 °C min^{-1} in a flowing atmosphere of air (30 cm^3 min^{-1}).

2.3. Catalytic activity

Ethanol was chosen as a probe molecule because it is an important VOC produced in fermentation and sponge dough processes and the industrial production of beer, food or pharmaceutical products [12].

Catalytic test was carried out at atmospheric pressure in a continuous flow tubular glass reactor. Two hundred milligrams of the sample were loaded in form of fine powder. The total gas flow of ethanol–air was 20 cm^3 min^{-1} and the work temperatures were between 100 and 300 °C. The feed composition was 900 ppm of ethanol in air, with an excess of O_2.

The reactants and the reaction products of a possible incomplete reaction were analyzed by using an on-line gas chromatograph (Shimadzu GC 8A, Porapak T for the analysis of ethanol, CO_2, acetaldehyde and a 5A zeolites for the analysis of CO) and quantified by using a TCD. For the purpose of comparison, the temperature at which the conversion of the organic compound reaches 50% (T_{50}) was used to analyze the activity of the catalysts in VOCs oxidation. The low T_{50} shows the best catalytic activity.

The adsorbed species formed during the reaction on the manganese oxides were studied by in situ DRIFT spectroscopy by using the same experimental conditions achieved in the studies of catalytic activity.

3. Results and discussion

X-ray diffraction was used to determine the bulk crystalline phases in the samples. The diffraction patterns of the manganese oxides are shown in Fig. 1. The XRD

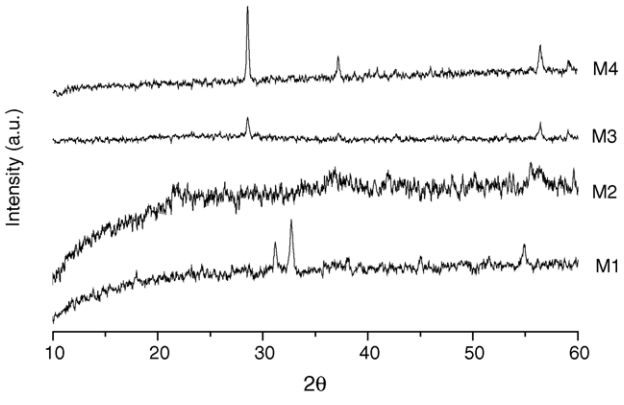

Fig. 1. X-ray powder diffraction patterns of the manganese oxides.

patterns of the commercial MnO_2 sample (M3) show the typical spectrum of β-MnO_2 phase (pyrolusite) (JCPDS, 24-0735). The oxide prepared by decomposition of $Mn(NO_3)_2{\cdot}4H_2O$ (M4) also shows the spectrum of pyrolusite.

A more complex XRD pattern is obtained for M1 sample. The signal at 2θ 33° indicates the presence of α-Mn_2O_3, bixbyite phase. Additionally, the broad and poorly resolved peak in the 2θ range 37–39° could indicate the presence of a mixture of Mn(IV) and Mn(III) oxides, according to Arena et al. [13]. Thus, this oxide is composed by a mixture of Mn_2O_3 and an amorphous Mn^{4+}–Mn^{3+} oxide.

Chabre and Pannetier [4] have reported that the XRD spectrum of the γ-MnO_2 (nsutite) phase is always of rather poor quality and consists, at best, of a small number of sharp and broad lines on top of a diffuse background. The X-ray powder diffraction pattern of M2 shows small and broad lines at 2θ 22°, 37°, 38° and 56°, which reveals the presence of the γ-MnO_2, according to database of the reference compound (JCPDS, 17-0510).

The BET specific surface areas of the samples are summarized in Table 1. The results showed a highest surface area for M2 sample (nsutite phase oxide). Its high surface area could be explained by a higher number of point defects on this oxide surface [14]. As it can be seen from the table, the M1 sample surface area is higher than that of M3 and M4, but lower than M2. Finally, although M4 and M3 present the pyrolusite structure, M4 has a 60 times higher surface area than M3.

The DRS–UV–vis position bands of different manganese oxides can be seen in Table 2. For the M3 and M4 samples, the spectra are characterized by an absorption band near 340 nm, which is assigned to Mn^{4+} [15]. The M1 and M2 samples also present that absorption. On the other hand, the spectrum of M1 and M2 samples presents an absorption band between 450 and 550 nm, which could be due to charge transfer transitions of octahedral Mn^{3+} [16]. These features suggest the existence of Mn^{4+} and Mn^{3+} in the bulk of the M1 and M2 oxides, in agreement with XRD data.

The results of DRIFT spectroscopy of the studied manganese oxides are reported in Table 3. Neither CO_3^{2-} nor SO_4^{2-} groups were detected by DRIFTS spectroscopy in the fresh catalysts.

IR spectroscopy has proven to be useful for the identification of the nsutite phases [17], and yields more reliable information than the X-ray diffraction technique. The IR bands in the region 1000–400 cm^{-1} reveal information about MnO_6 octahedra [18]. Moreover, Potter and Rosmann [19] stated that the infrared spectroscopy is sensitive to octahedral polymerization. Besides, Julien et al. [20] observed a general decrease in band wavenumber with increasing octahedral polymerization. These author assigned the bands at 545 cm^{-1} in pyrolusite and at 522 cm^{-1} in ramsdellite to the vibration due to the displacement of the oxygen anions relative to the manganese ions along the direction of the octahedral chains.

Table 2
DRS–UV–vis bands of manganese oxides

Sample	Mn^{4+} (nm)	Mn^{3+} (nm)
M1	450–550	340
M2	450–550	340
M3	450–550	
M4	450–550	
Mn_2O_3		340

Table 3
IR frequency vibration of manganese oxides

Sample	IR bands (cm^{-1})			References
M1	727	633	544	
M2	718	633	542	
M3	–	616	560	
M4	–	615	560	
β-MnO_2		618	562	[19,20]
R-MnO_2	743	649, 630	522	[19,20]
R-MnO_2	740	687	529	[19]
γ-MnO_2	705		545	[19]

The M1 bands at 727 and 544 cm^{-1} could be assigned to γ-MnO_2 and the band at 633 cm^{-1} to Mn_2O_3, respectively. In the case of M2, DRIFTS bands are in accordance with those reported by Potter and Rossman [19] for the γ-MnO_2 phase. In addition, these authors have also reported that the characteristic bands of ramsdellite are at 522, 630, 649 and 743 cm^{-1}. Taking into account the correlation of infrared spectra made by Potter and Rossman [19] and Julien et al. [20], it is possible to determine the structural characteristics of our manganese oxides (M1, M2). In Fig. 2, the positions of the IR bands are shown as a function of edge shared octahedra. Both M1 and M2 samples are placed between the ramsdellite and the pyrolusite, in agreement with the fact that the γ-MnO_2 is a mixture of ramsdellite and pyrolusite structures [3].

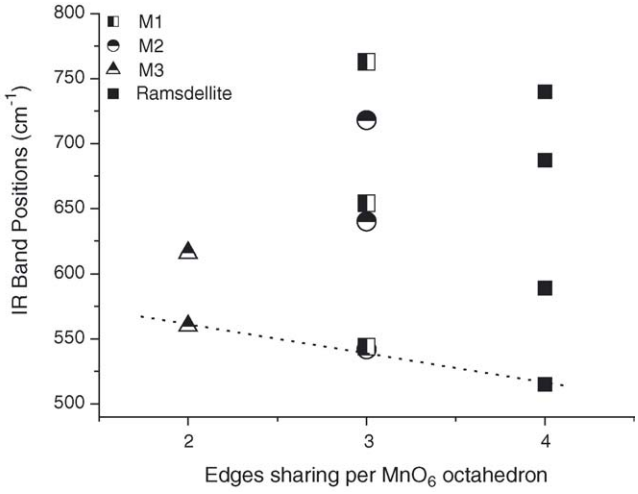

Fig. 2. Frequency positions of the IR bands, a function of the average MnO_6 octahedral polymerization in manganese oxides. (ramsdellite bands, Potter and Rosmann [18]).

According to the results of the characterization techniques we can say that:

(a) M1 catalysts are constituted by an amorphous mixed Mn_2O_3–γ-MnO_2 oxide.
(b) M2 is an oxide of the γ-MnO_2 (nsutite) type with manganese(III) and manganese(IV) cations.
(c) M3 and M4 catalysts have the β-MnO_2 (pyrolusite) structure and the manganese oxidation state is IV in both catalysts.

Kanungo et al. [21] have reported that the thermal analysis of manganese oxides between 25 and 900 °C in air presents three different thermal effects: (a) loss of physically adsorbed molecular water in the temperature range 100–200 °C; (b) loss of chemically bound water and a change of crystalline phase between 200 and 400 °C; and (c) the transformation of MnO_2 to Mn_2O_3 around 550 °C. Likewise, Vileno et al. [22] in their studies of OMS manganese oxides also reported three thermal events: loss of physisorbed water from 100 to 130 °C; loss of chemisorbed water, inside or outside the tunnels, at 200 °C; and loss of oxygen.

Fig. 3 depicts TG curves for the studied oxides except for M4. As it can be seen, decomposition of MnO_2 to Mn_2O_3 in M1 sample occurs at 580 °C. The other catalysts show a completely different behaviour. In fact, M2 sample is still losing water even at 800 °C. This is in agreement with Petit et al. [23] who pointed out that the γ-MnO_2 is non-stoichiometric unless the temperature is raised up to 800 °C. This is due to the presence of OH-groups in the bulk of the oxide. They have also shown that this oxide presents electrochemical activity at temperatures higher than 450 °C. Finally, M3 is the most stable oxide. There is not physically or chemically bound water, since no weight loss is present until the temperature reaches 610 °C. At this stage, the transformation to Mn_2O_3 occurs with approximately 10% weight loss, and it is in agreement with the calculated value (9.2%).

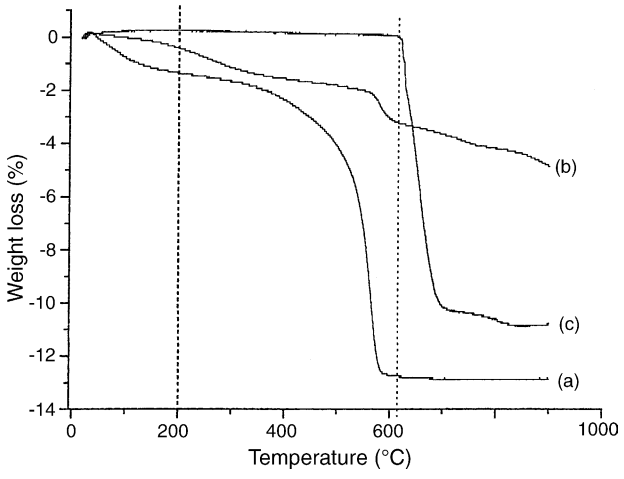

Fig. 3. TGA curves for manganese oxides: (a) M1; (b) M2; (c) M3.

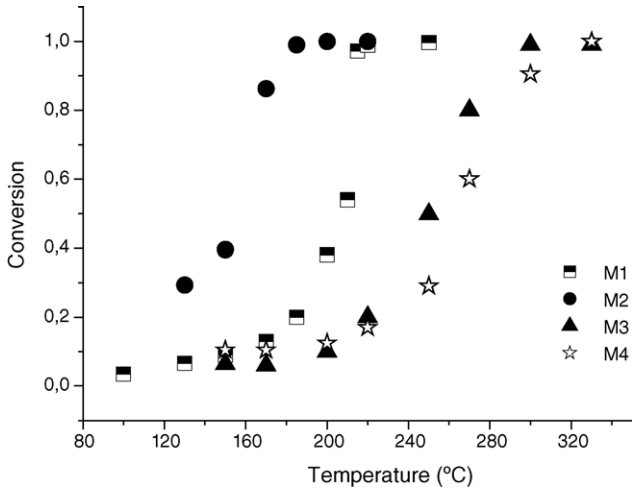

Fig. 4. Total ethanol conversion as function of temperature.

The catalytic performances for ethanol oxidative destruction on manganese oxide catalysts are shown as function of temperature in Fig. 4. In all the samples tested, CO_2, H_2O and acetaldehyde were formed during ethanol oxidation, and no other partial oxidation products were detected. Preliminary experiments showed that the commercial manganese carbonate did not exhibit any activity at all for the catalytic oxidation of ethanol.

Fig. 4 shows that the oxide with the nsutite structure (M2 sample) is a more active catalyst with a T_{50} more than 40 °C lower than that of the catalyst prepared by decomposition of $MnCO_3$ (M1 sample). Total combustion occurs at 200 °C for the M2 catalyst, and at around 215 °C for M1 catalysts. In both catalysts (M1 and M2), the selectivity to acetaldehyde was at a peak when the conversion was low (less than 20%). It was also observed that carbon dioxide was the only product, when the conversion reached 30%. Both pyrolusite type catalysts (M3 and M4) have the lowest activity of the catalysts with a T_{50} close to 250 °C. The combustion is not total until the temperature reaches 300 °C.

As we have seen, the most crystalline and lowest specific surface area oxide (M3, β-MnO_2) has the lowest activity, and the most active catalyst (M2) has the lowest crystallinity and the highest specific surface area. These results are in agreement with Stobbe et al. [24] and Shaheen and Selim [25], who have reported that the oxides with high degree of crystallinity had a pronounced decrease in catalytic activity.

Nevertheless, not only the surface area but also the structure of the oxides influences in the catalytic activity of this series of oxides. M4 sample has a 60 times higher specific surface area than that of M3 sample (Table 1), but the activity of the former is lower than that of the latter (see Fig. 4).

Besides the specific surface area and the crystallinity of the catalysts, the existence of the Mn^{3+}–Mn^{4+} couple [26–28], the presence of cationic vacancies and OH groups [29] are responsible for the high activity achieved by the nsutite-phase oxide (M2).

As far as the oxidation state is concerned, the UV–vis and DRIFTS spectra showed that M1 and M2 samples contained Mn^{3+} and Mn^{4+} ions, whereas pure MnO_2 without any amount of Mn^{3+} constituted M3 and M4 samples. Although both M1 and M2 samples contain Mn^{3+} in their structure, they have different crystalline structures. In M1 sample, Mn^{3+} is present in the form of crystalline Mn_2O_3 and it is also present in a mixed Mn^{4+}–Mn^{3+} amorphous oxide, where the presence of the Mn^{4+} ions could be associated with γ-MnO_2 phase. But in the case of M2 sample, Mn^{3+} cations could be distributed in a nsutite matrix replacing Mn^{4+} cations. In this oxide, no Mn_2O_3 is detected.

Taking into account the catalytic activity results, oxides with Mn valence between 3 and 4 were more active than those with pure Mn (+4). M1 catalyst had a mixed structure of Mn_2O_3 and γ-MnO_2, as it was confirmed by DRIFTS spectra. Therefore, the presence of the couple Mn^{3+}–Mn^{4+} could be responsible for the best catalytic performances compared to β MnO_2 and synthetic Mn_2O_3 [8].

The presence of Mn^{4+} vacancies in the nsutite structure is followed by the formation of OH groups, in order to equilibrate charges. The TGA results showed OH species at 200 °C when conversion was complete for M2. So, we can say that OH groups played an important role in the oxidation mechanism of VOC's.

Fig. 5 shows the DRIFTS spectra of adsorbed species over M1 catalysts. The spectrum of ethanol adsorption over M1 sample from RT to 70 °C shows bands assigned to ethoxide species (1640–1650 cm^{-1} enolic anion; 1420 cm^{-1} δ_{OH}; near 1110 cm^{-1} C–O stretching and 1050 cm^{-1} ethoxy group) [30,31]. At 70 °C, a new band at 1746 cm^{-1} attributed to vibration $\nu_{C=O}$ (acetaldehyde) is detected. At 150 °C, bands begin to be formed at 1430 and 1555 cm^{-1}, that can be assigned to a chelate bidentate acetate [29]. Above 150 °C, three bands are detected, two of them (1425–1570 and 1045 cm^{-1}) assigned to bridged bidentate acetate and at 1350 cm^{-1}, a third band attributed to the monodentate acetate species. The fact that different organic species are found in M1 enables us to suppose that there are two different mechanisms of adsorption-reaction, in good agreement with Batiot and Hodnett [32] and Blasim-Aubé et al. [33], who have postulated that the ethanol oxidation to carbon dioxide over catalyst can be described as:

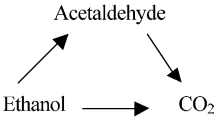

Then, the formation of different adsorbed species could depend upon the different bond dissociation enthalpy of the weakest C–C and C–H bonds that ethanol and acetaldehyde (389 kJ/mol C–H ethanol, 358 and 349 kJ/mol C–C and C–H acetaldehyde) present when they are oxidized to CO_2.

Fig. 6 shows the infrared spectra of the adsorbed species over M2 as a function of the reaction temperature. The spectrum is different from the one recorded over M1 sample. At room temperature, bands are detected at: (i) 1290 cm^{-1} attributed to adsorbed ethanol; (ii) 1023 cm^{-1} assigned to ethoxy species; and (iii) 1475 cm^{-1} corresponding to a vibration δ_{CH_2}. In the range 70–200 °C, the main bands are detected at: (i) 1270–1500 cm^{-1} attributed to monodentade carbonate; and (ii) 1736 cm^{-1} assigned to carbonyl species (acetaldehyde). In addition, the shoulder at 1177 cm^{-1} could be due to ethoxy species coordinated over metal sites.

These results showed that the adsorption-reaction pathway of ethanol over M2 was produced by the presence of different adsorbed species with respect to M1 catalyst.

Taking into account these results, we propose the following pathways for ethanol oxidation:

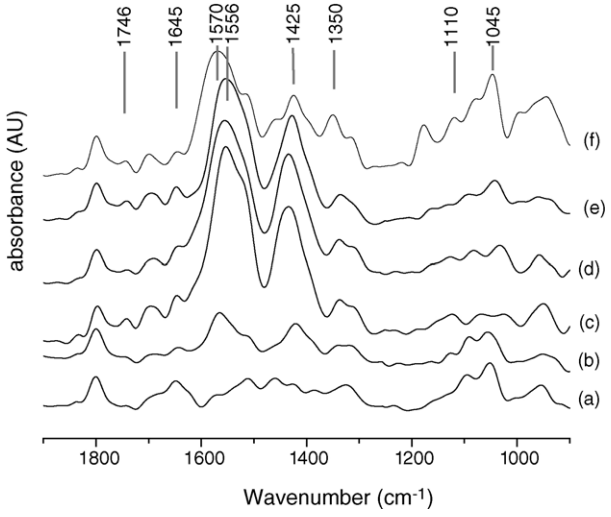

Fig. 5. In situ DRIFTS spectra of the adsorption of ethanol on M1 catalyst as a function of the temperature: (a) RT; (b) 70 °C; (c) 100 °C; (d) 120 °C; (e) 150 °C; (f) 200 °C.

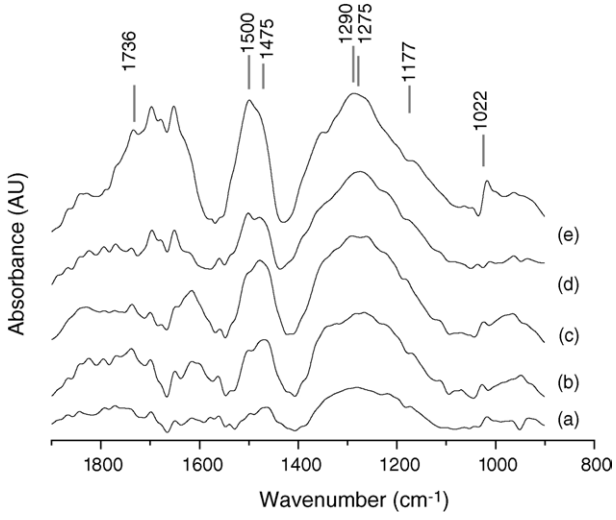

Fig. 6. In situ DRIFTS spectra of the adsorption of ethanol on M2 catalyst as a function of temperature: (a) RT; (b) 70 °C; (c) 100 °C; (d) 150 °C; (e) 200 °C.

over M1 catalysts

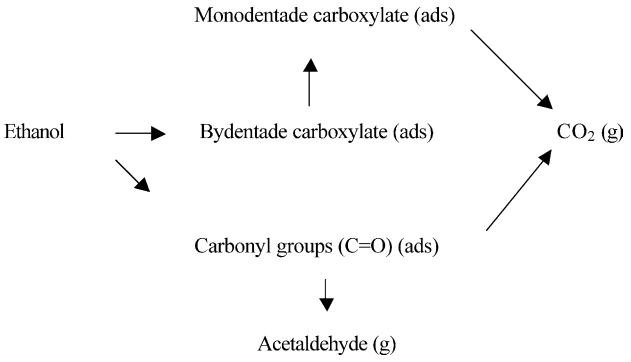

and over M2 catalysts

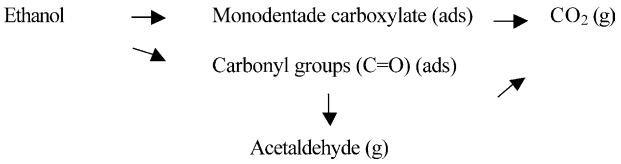

The different mechanism could be attributed to the formed solid. According to Ruetschi [34], γ-MnO_2 contains Mn vacancies compensated by four protons that are attached to the vacancy (OH formation). So, the interaction between ethanol and oxygen and/or hydroxyl centres on the surface of M2 catalyst could favour the formation of monodentade carboxylate species and improve the catalytic performances.

4. Conclusions

Two manganese oxides were synthesized in order to obtain the nsutite phase (γ-MnO_2) and to make a comparison with two dioxides with the pyrolusite structure (β-MnO_2). The oxides with the nsutite (γ-MnO_2) structure (M2 and M1) are more active catalyst than the solids with pyrolusite structure (β-MnO_2, M3 and M4).

The characterization results allow us to conclude that the high activity of both catalysts could be due to its poor crystallinity, the existence of the couple Mn^{3+}–Mn^{4+} and the presence of Mn^{4+} vacancies.

The in situ DRIFT spectroscopy showed that the two synthetic manganese oxides presented different mechanisms of adsorption-reaction of ethanol.

The mechanism of adsorption and the changes in the activity between M1 and M2 catalysts could be explained when assuming that these catalysts contain different structures: Mn_2O_3/γ-MnO_2 and γ-MnO_2, respectively.

Acknowledgments

The authors acknowledge Prof. L. Cadús (UNSL, Argentina) for TGA analysis, and Prof. G. Minnelli (U. La Sapienza, Italy) for the DRS–UV–vis spectra. M. Peluso thanks Comisión de Investigaciones Científicas of Buenos Aires (Argentina) for his Ph.D. fellowship.

References

[1] Baur, Acta Cryst. 32 (1976) 2200.
[2] T. Moore, M. Ellis, P. Selwood, J. Am. Chem. Soc. 72 (1950) 856.
[3] P. de Wolff, Acta Cryst. 12 (1959) 341.
[4] Y. Chabre, J. Pannetier, Prog. Solid State Chem. 23 (1995) 1.
[5] L. MacLean, Ch. Poinsignon, J. Amarilla, F. Le Cars, P. Strobel, J. Mater. Chem. 5 (1995) 1183.
[6] F. Volkenshtein, The Electronic Theory of Catalysis on Semiconductors, Pergamon Press, New York, 1963.
[7] C. Lahousse, A. Bernier, E. Gaigneaux, P. Ruiz, P. Grange, B. Delmon, Third World Congress on Oxidation Catal, 1997, p. 777.
[8] M. Peluso, J. Sambeth, H. Thomas, React. Kinet. Catal. Lett. 80 (2003) 241.
[9] S. Netto, R. Hypolito, J. Valarelli, R. Giovanoli, R. Shultz-Gütler, An. Acad. Bras. Cienc. 70 (1998) 563.
[10] J. Fernández, B. Desai, K. Dalal, J. Power Sources 15 (1985) 209.
[11] Join Committee on Powder Diffraction Standard, JCPDS Files, International Centre of Diffraction Data, 2000.
[12] A. Buonicore, W. Davids (Eds.), Air Pollution Engineering Manual, Air and Waste Management Association, 1992.
[13] F. Arena, T. Torre, C. Raimondo, A. Parmaliana, Phys. Chem. Chem. Phys. 3 (2001) 1911.
[14] J. Boyero Macstre, E.F. López, J. Gallardo Amores, R. Ruano Casero, V. Sánchez Escribano, E. Pérez Bernal, Inorg. Mater. 3 (2001) 889.
[15] F. Millela, J. Gallardo Amores, M. Baldi, G. Busca, J. Mater. Chem. 8 (1998) 2525.
[16] A. Lahousse, P. Bernier, P. Grange, B. Delmon, P. Papaefthimou, T. Ioannides, X. Verykiost, J. Catal. 178 (1998) 214.
[17] C. Julien, M. Massot, J. Power Sources 119–121 (2003) 743.
[18] M. Ananth, S. Pethkar, K. Dakshinamurthi, J. Power Sources 75 (1998) 278.
[19] R. Potter, G. Rosmann, Am. Mineral. 64 (1979) 1199.
[20] C. Julien, M. Massot, C. Poinsignon, Spectroch. Acta A 60 (2004) 689.
[21] S. Kanungo, J. Catal. 58 (1979) 419.
[22] E. Vileno, Y. Ma, H. Zhou, S. Suib, Microporous Mesoporous Mater. 20 (1998) 3.
[23] F. Petit, J. Dürr, M. Lenglet, B. Hannoyer, Mater. Res. Bull. 28 (1993) 959.
[24] E. Stobbe, B. de Boer, J. Geus, Catal. Today 47 (1999) 161.
[25] W. Shaheen, M. Selim, Thermochim. Acta 332 (1998) 117.
[26] K. Parida, S. Kanungo, Thermochim. Acta 64 (1983) 131.
[27] N. Deraz, M. El-Sayed, A. El-Alal, Adsorption Sci. Technol. 19 (2001) 541.
[28] M. Galván, P. O'Shea, J. Fierro, P. Arias, Catal. Commun. 4 (2003) 223.
[29] P. Ruetschi, R. Giovanoli, J. Electrochem. Soc. 135 (1988) 2663.
[30] W. Chun, C. Chuang, J. Lin, J. Phys. Chem. B 104 (2000) 8719.
[31] K. Nakamoto, Infrared and Raman Spectra of Inorganic and Coordination Compounds, fifth ed., Wiley & Son Inc., New York, 1997.
[32] C. Batiot, B. Hodnett, Appl. Catal. A 137 (1996) 179.
[33] V. Blasim-Aubé, J. Belkouch, A. Monceaux, Appl. Catal. B 43 (2003) 175.
[34] P. Ruetschi, J. Electrochem. Soc. 131 (1984) 2737.